Article

Energy Saving for Impinging Jet Ventilation System by Employing Various Supply Duct Locations and Return Grill Elevation

Bandar Awadh Almohammadi [1] , Eslam Hussein [2] , Khaled M. Almohammadi [3] , Hassanein A. Refaey [1,2,*] and Mohamed A. Karali [4,*]

1   Department of Mechanical Engineering, College of Engineering at Yanbu, Taibah University, Yanbu Al-Bahr 41911, Saudi Arabia
2   Department of Mechanical Engineering, Faculty of Engineering at Shoubra, Benha University, Cairo 11629, Egypt
3   Department of Mechanical Engineering, College of Engineering at Madinah, Taibah University, Al-Madinah Al-Munawara 42353, Saudi Arabia; kalmohammadi@taibahu.edu.sa
4   Department of Mechanical Engineering, Faculty of Engineering and Technology, Future University in Egypt, New Cairo 11835, Egypt
*   Correspondence: hassanein.refaey@feng.bu.edu.eg (H.A.R.); mohamedkarali@yahoo.com or mkarali@fue.edu.eg (M.A.K.)

Abstract: The study of energy savings in ventilation systems within buildings is crucial. Impinging jet ventilation (IJV) systems have garnered significant interest from researchers. The identification of the appropriate location for the IJV reveals a gap in the existing literature. This research was conducted to address the existing gap by examining the impact of IJV location on energy savings and thermal comfort. A comprehensive three-dimensional CFD model is examined to accurately simulate the real environment of an office room ($3 \times 3 \times 2.9$ m^3) during cooling mode, without the application of symmetrical plans. Four locations have been selected: two at the corners and two along the midwalls, designated for fixed-person positions. The return vent height is analyzed utilizing seven measurements: 2.9, 2.6, 2.3, 1.7, 1.1, 0.8, and 0.5 m. The RNG k–ε turbulence model is implemented alongside enhanced wall treatment. The findings indicated that the optimal range for the return vent height is between 1.7 and 0.8 m. It is advisable to utilize the IJV midwall 1 location, positioned behind the seated individual and away from the exterior hot wall. It is characterized by low vortex formation in the local working zone that contributes to a more comfortable sensation while providing recognized energy-saving potential.

Keywords: HVAC; impinging jet ventilation; thermal comfort; indoor air quality; energy saving; office building; CFD

1. Introduction

Since energy consumption emerged as a global environmental and economic issue, scientists have diligently sought methods to save energy. The air conditioning of buildings accounts for a significant portion of global energy consumption [1]. Consequently, significant emphasis has been placed on energy conservation for this air conditioning units, commencing with the chosen ventilation system method to the air conditioning coil apparatus itself. Various ventilation systems are identified and implemented in practice. The conventional system is the mixing ventilation (MV) system, referred to as the "overhead ventilation system". It provides improved temperature homogeneity inside the space but with significant energy consumption. Additional advanced systems include the displacement ventilation (DV) system, the underfloor air distribution (UFAD) system, and the impinging jet ventilation (IJV) system. The final three varieties provide a nonuniform temperature environment inside the conditioned room, exhibiting significant temperature

stratification; however, they are more energy-efficient compared to the conventional mixing type [2,3]. The current investigation will concentrate on the IJV system; further information about this kind will be provided thereafter. Karimipanah and Awbi [4] advocated using this ventilation system in office, school, and industrial settings. The first studies were conducted by Awbi [5], Rohdin and Moshfegh [6], Varodompun [7], and Chen et al. [8]. In an IJV, a high-velocity air jet is emitted at a specified height, subsequently striking the floor and scattering over it, distributing fresh air in a thin layer across the surface. The IJV maintains the advantages of the DV while mitigating the drawback of its limited momentum provision. Displacement ventilation (DV) is acknowledged for its superior ventilation efficiency, enhanced by the notion of stratification [9,10]. IJV may thus provide superior ventilation for work areas compared to DV since the air it delivers has sufficient velocity to overcome the buoyancy force generated by heat sources and reach other regions of the room. A plethora of studies in the literature examine several significant elements of IJV systems, as outlined below. Chen et al. [11] conducted research on the configuration of the supply device for an IJV system with a discharge height of 0.6 m under isothermal conditions. The research indicated that the configuration of the supply diffuser significantly affects the flow pattern on the floor. Varodompun and Navvab [12] also investigated other parameters, such as thermal load and air supply outlet dimensions. Previous research by Awbi [4] and Chen et al. [11] showed that the most significant reduction in jet velocity and temperature distribution is somewhat affected by the discharge height. Nevertheless, the effect on thermal comfort and indoor air quality (IAQ) was found to be greater than first anticipated.

Numerous studies [13,14] have proposed using a discharge height of 0.4 m from the floor. Chen et al. [15] evaluated the flow and temperature distribution inside an office environment with IJV under different thermal loads. The IJV system was evaluated with a chilled ceiling system to address both cooling requirements and heating demands for the floors. The study findings demonstrated that modifying various setup parameters to enhance air circulation led to a decrease in temperature stratification within the area. This may be ascribed to the improved entrainment of the provided air. Cehlin et al. [16] evaluated the efficacy of air circulation in an office space fitted with an IJV system and a cooled ceiling. The assessment was performed under different thermal loads while the room operated in cooling mode. The research by Staveckis and Borodinecs [13] sought to evaluate the efficacy of IJV throughout different climatic conditions, encompassing summer and winter, alongside various human postures within office environments and distinct geometrical configurations of the input supply. The study's results indicated that IJV was appropriate for summer cooling and winter heating. The study's results suggested that IJV demonstrated much higher ventilation efficiency than mixed ventilation.

Cheng et al. [17] proved that, in a well-designed mixed ventilation system, the positions of return and exhaust inlets do not significantly affect the cooling coil load, since the room temperature remains consistent. However, unlike the IJV system, the pronounced thermal stratification of interior air significantly influences the cooling coil load based on the placement of return and exhaust grills. Numerous studies indicated that separating exhaust and return vents, rather than merging them, was more advantageous for energy conservation [18]. All research asserted that the optimal position for the exhaust was the ceiling exhaust, situated near the heat plume originating from the working zone. Positioning the ceiling exhaust nearer to the thermal plume enhanced heat removal efficiency and improved thermal comfort, namely by lowering temperature and *PMV* [19,20]. Researchers have shown that a return vent situated above 2.3 m offers little enhancement to energy efficiency; however, a return vent placed below 0.8 m resulted in thermal discomfort owing to short circuits [21]. Table 1 summarizes the most relevant research pertaining to this subject.

Table 1. Related research summary.

Research Authors	Year	System	Scope of Studying
Cheng et al. [17]	2016	UFAD	return vent height
Ahmed et al. [19]	2016	DV	exhaust locations
Fan et al. [21]	2017	UFAD	return vent height
Haghshenaskashani et al. [18]	2018	IJV	return vent height with/without ceiling exhaust
Qin and Lu [22]	2021	IJV	ceiling exhaust location
Qin et al. [20]	2022	IJV	optimization on return vent height

IJV: impinging jet ventilation; DV: displacement ventilation; UFAD: underfloor air distribution.

A variety of CFD studies exist in the literature that examine suitable turbulence models for IJV studies. Four models—standard k–ε, RNG k–ε, realizable k–ε, and SST k–ω—have been commonly utilized in research related to IJV systems [11,15,23–26]. These models were selected due to their superior performance in predicting impinging jet airflow and temperature distributions. Recent literature surveys by Ameen et al. [27], Ameen et al. [28], and Yang [29] on turbulence models for IJV studies recommended the use of the RNG k–ε model with the IJV systems. Thus, the RNG k–ε model was determined to be the most effective among the other models analyzed in comparison to experimental results.

Most research on IJV has primarily focused on a centrally located discharge inlet within a wall. The corner IJV position has been utilized in numerous studies [27,28]. There exists limited research investigating the effects of altering the placement of the IJV on thermal comfort and indoor air quality, accompanied by detailed information. Yamasawa et al. [30] conducted a study comparing center- and corner-positioned internal jugular veins (IJVs). The findings indicated that the efficiency of cooling and ventilation in the room may be improved by placing the supply terminal at the midpoint of the walls instead of in the corner.

In conclusion, there is a lack of significant studies examining the impact of IJV location on thermal comfort, indoor air quality, and energy savings. Thus, the present study was planned to fill this gap. A comprehensive 3D CFD model is examined to accurately simulate the real environment of an office room ($3 \times 3 \times 2.9$ m^3) during cooling mode, without the application of symmetrical plans. Four locations have been selected for the IJV: two at the corners and two along the midwalls, designated for fixed-person positions. The return vent height is analyzed utilizing seven measurements: 2.9, 2.6, 2.3, 1.7, 1.1, 0.8, and 0.5 m. Meanwhile, the exhaust vent location is maintained at the center of the ceiling, as recommended by the literature. This article, alongside existing literature, offers valuable insights for HVAC designers in this field of study. All the method details and results will be shown in the following.

2. Methods

2.1. Geometrical Parameters and Studied Domains

Figure 1 illustrates the simulated office room in the present CFD study, which has a floor area of 3×3 m^2 and a height of 2.9 m. The room simulates a real office environment, featuring one workplace equipped with a seated thermal manikin, a chair, a desk, a personal computer, and a cupboard. Two lighting systems have been installed in the ceiling. The room features a single side wall, which contains a glass window with an area of 1 m^2, oriented towards the external ambient conditions of the building's exterior. The window is assumed to have a transmissivity of 0.5. The five internal walls, along with the floor and ceiling, interface with the environment of the adjacent room, which is presumed to be air-conditioned. The walls of the room consist of brick with a thickness of 10 cm. The IJV system air inlet height is maintained at 0.4 m above the floor, following recommendations from prior studies [13,14]. The current study identifies four distinct locations within the IJV system, selected for their significant purposes, including aesthetic decoration and effective interior design. These locations comprise two corners and two midwalls, designated for a fixed-person position: corner 1 (posterior to the manikin), corner 2 (anterior to the manikin),

midwall 1 (posterior to the manikin), and midwall 2 (lateral to the manikin). This study positions the exhaust grill at the center of the ceiling, situated between the two lighting systems, as discussed in the introduction regarding optimal placement. The return grill is positioned on the wall opposite the hot exterior wall. The current research examines seven selected return vent heights: 0.5, 0.8, 1.1, 1.7, 2.3, 2.6, and 2.9 m from the floor to achieve meaningful results. A total of twenty-eight simulations are configured and analyzed in this research, incorporating four locations of the IJV and seven locations of the return vent heights, with detailed specifications provided in Table 2.
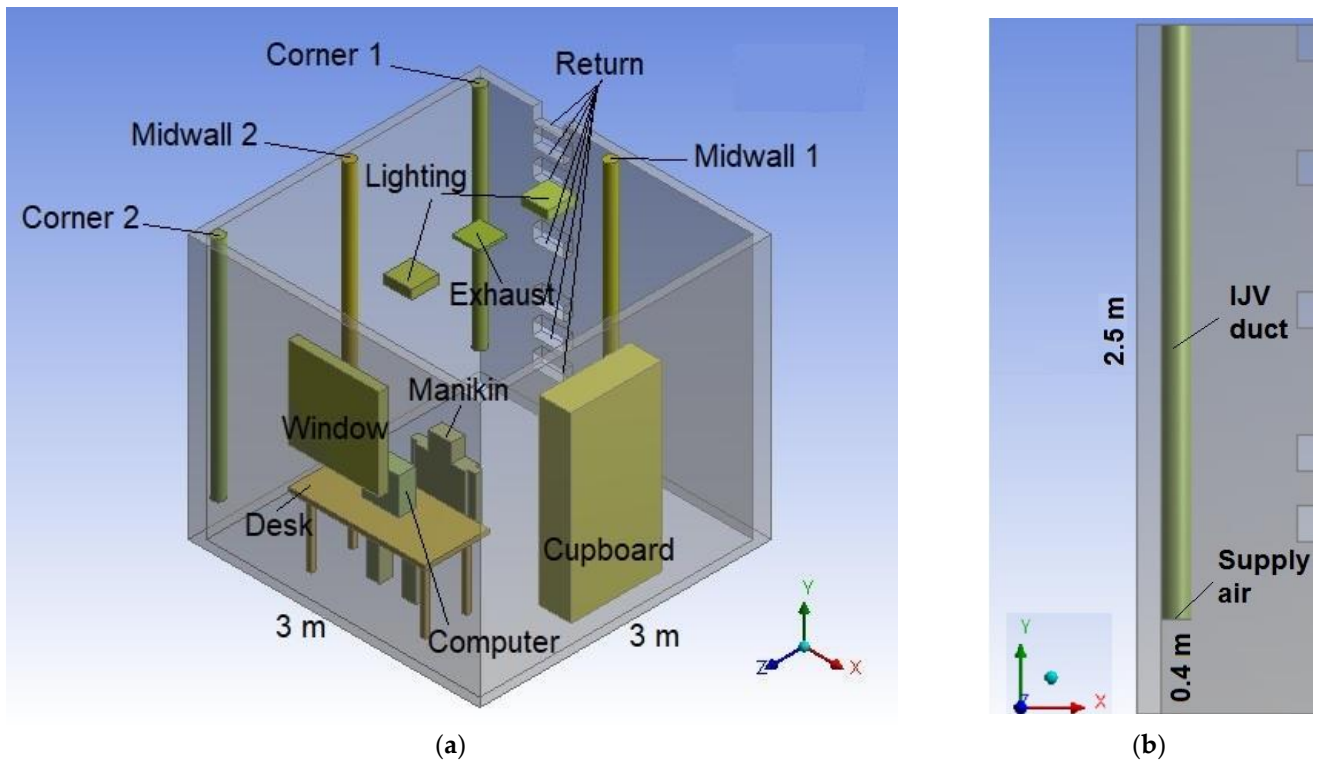

(**a**)   (**b**)

Figure 1. (**a**) Simulated office with an impinging jet ventilation system at different locations, showing different return vent heights; (**b**) side view of the IJV system showing the height from the floor.

Table 2. Specifications of simulations.

No.	Simulation Code	Supply Duct Location	Return Height (m)	No.	Simulation Code	Supply Duct Location	Return Height (m)
1	c2rH2.9		2.9	15	c1rH2.9		2.9
2	c2rH2.6		2.6	16	c1rH2.6		2.6
3	c2rH2.3		2.3	17	c1rH2.3		2.3
4	c2rH1.7	Corner 2	1.7	18	c1rH1.7	Corner 1	1.7
5	c2rH1.1		1.1	19	c1rH1.1		1.1
6	c2rH0.8		0.8	20	c1rH0.8		0.8
7	c2rH0.5		0.5	21	c1rH0.5		0.5
8	mw2rH2.9		2.9	22	mw1rH2.9		2.9
9	mw2rH2.6		2.6	23	mw2rH2.6		2.6
10	mw2rH2.3		2.3	24	mw1rH2.3		2.3
11	mw2rH1.7	Midwall 2	1.7	25	mw1rH1.7	Midwall 1	1.7
12	mw2rH1.1		1.1	26	mw1rH1.1		1.1
13	mw2rH0.8		0.8	27	mw1rH0.8		0.8
14	mw2rH0.5		0.5	28	mw1rH0.5		0.5

c: corner; mw: midwall; rH: return height.

2.2. Boundary Conditions

The present study is designed to test the previously described office room in Section 2.1 under summer season conditions of a hot outdoor climate. The outdoor conditions are taken to be at 38 °C dry-bulb temperature, and with 700 W/m^2 solar heat flux intensity. Therefore, a cooling process for this hot air is essentially required to achieve the desired comfort conditions inside the office room. While the inlet-supplied air conditions that come out from the IJV system are assumed to be constant at 20 °C (dry-bulb temperature) and 75 m^3/h air flow rate, different IJV system locations and return vent heights are tested in this study, as listed earlier in Table 1. It is worth noting that this supplied air temperature (20 °C) is selected after several trials based on the assumed outdoor temperature (38 °C) and other pre-described room conditions, targeting to achieve a suitable average operative temperature, besides energy saving as possible. In this study, the average operative temperature is assumed to be between 24 °C to 26 °C and with 50% relative humidity, which matches ASHREA 55 standards [31]. Table 3 summarizes all the room operating conditions. The IJV inlet to the room (supply air) is defined as a velocity inlet with constant temperature. The exterior surface of the room's wall that contains the window is assumed to be at the same constant temperature as the outdoor conditions. The remaining five internal walls including the floor and ceiling are assumed to be adiabatic with no heat transfer along with the next environments. Air return out from the room is defined as an outlet with a predefined velocity based on the return air ratio from the supplied air (83%). Air exhaust from the room is defined as an outlet with zero pressure. The internal loads inside the room are taken as found in Table 4, for the manikin (125 W), the two lighting systems (100 W), and the computer (60 W), with a total of 285 W internal heat load.

Table 3. Room operating conditions.

Condition	Value
Supply air temperature	20 °C (dry-bulb)
Supply air flow rate	75 m^3/h
Return air ratio	83%
Operative air temperature	24–26 °C
Operative relative humidity	50%
Outdoor air temperature	38 °C (dry-bulb)
Solar heat flux intensity	700 W/m^2

Table 4. Room internal heat loads.

Heat Source	Heat Load in W
Manikin	125
Lighting	2 × 50
Computer	60
Total	285

2.3. Turbulence Model Selection and Equations

Based on the previous literature discussion about suitable turbulence models, the present study utilizes the Reynolds-averaged Navier–Stokes equations (RANS) and employs the RNG k–ε two-equations turbulence model. The ANSYS-CFX R18.0 CFD solver code is being used in this work. The airflow and temperature in the model are described by the conservation laws of mass, momentum, and energy equations. The buoyancy effect is included in the momentum equation and the Boussinesq approximation was used. The simulations were performed with the following assumptions and limitations: three-dimensional, steady-state (all the states of the dynamic system have reached an equilibrium state), incompressible, and turbulent conditions. A full description of the equation system is found in Karali et al. [32], ANSYS CFX R18.0 [33], and Ameen et al. [27]. The model chosen for radiation heat transfer is the Discrete Transfer model. The "SIMPLE" pressure–velocity

coupling technique was employed. The second-order upwind discretization strategy was employed for the pressure, momentum, turbulent kinetic energy, and particular dissipation rates. The solution was declared converged when the residual was attained less than 10^{-4} for energy and 10^{-6} for other parameters. The solution convergence criterion employed was the residual mean square type (RMS). It is noteworthy to mention that all the simulations conducted were executed without the utilization of any symmetry plane to match the real building environment.

2.4. Meshing Specifications and Independence Study

In the present CFD study, a non-uniform grid spreading was employed using ANSYS-ICEM Mesh R18.0 [33], with a refinement for the mesh staying focused on and around the inlet, walls, and objects in the room. Ten layers were adopted with a first-layer thickness of 0.08 mm and an inflation rate of 1.2. Figure 2 shows an overview of the mesh configuration in the computational domain with a zoom-in view of the wall layers for the case of corner 1 IJV.
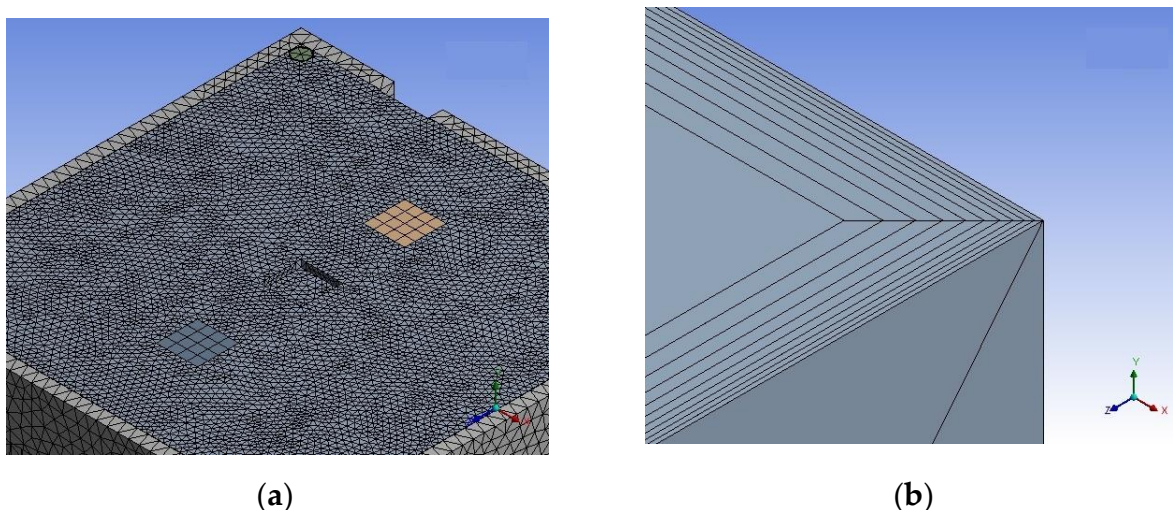

(a)   **(b)**

Figure 2. (**a**) Overview from the meshing in the computational domain for the case of corner 1 IJV location; (**b**) zoom-in view from the wall layers.

To obtain a good solution from CFD, a mesh independent study has been employed for the current study. Therefore, in the study, to select the suitable mesh to be used, five discrete mesh densities were assessed and compared from the case of midwall 1, so that a condensed mesh was adapted near the walls to capture the results. The selection criterion is based on measuring the fluid velocity at different heights from floor to ceiling on a vertical centerline inside the room. The number of elements used is 333,680, 1,234,967, 2,069,919, 3,912,266, and 8,931,279, respectively. The deviations of these measurements are found as 10.36, 4.37, 0.89, and 1.9%, respectively. Thus, mesh 4 is found to record the minimum deviation among the tested meshes. Thereafter, mesh 4 with 3,912,266 elements was used for the currently studied simulations.

2.5. Model Validation with Experimental Data

The current CFD model specifications are validated with available experimental results from related literature found in Ameen et al. [28]. In their experimental work, the IJV duct was placed in the room corner and of triangle-shaped inlets with the following configurations: the inlet area for each inlet was set to 0.0133 m^2 with the side dimensions of 163 × 163 × 231 mm. The supply air temperature was maintained at 17 °C and the flow rate for each inlet was set to 10 L/s (20 L/s in total), for an assumed outdoor temperature of 20 °C, while adiabatic walls are assumed for all internal walls. The exhaust outlet is located in the ceiling near the opposite wall. The manikins used in the experiments had

the same surface area as a human, and each produced 100 W of heat in a sitting position. Two enclosures containing a halogen lamp generated 75 W of heat each when used in the experiment, which were placed at the side of each desk. The validation was performed based on using the RNG k–e turbulence model and all measurements were taken at the center point of the room. Figure 3 shows a comparison between the experimental and CFD results from Ameen et al. [28], works, and the present model predictions. The results show that the predicted temperature and velocity profiles exhibit good consistency.
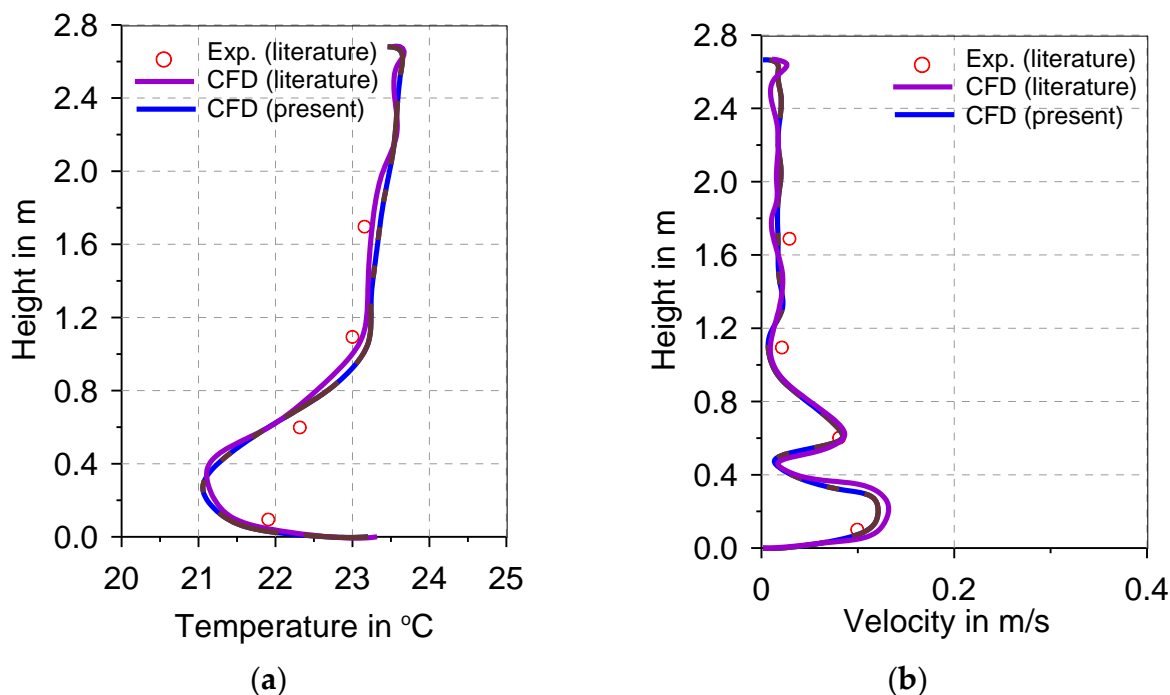
Figure 3. CFD model validation with experimental results. (**a**) Temperature profile, and (**b**) velocity profile.

3. Evaluation of Energy Saving

In this study, the energy saving of the used system is evaluated using the energy saving potential term (ΔQ_{coil}), where the notation "coil" denotes the coil of the used device for the cooling or heating processes, e.g., the air handling unit coil. This choice is based on the fact that the coil load is directly proportional to the device energy consumption at a certain coefficient of performance (*COP*). Hence, it well represents the energy saving. ΔQ_{coil} expresses the difference between this coil load when using the impinging jet ventilation system (*IJV*) rather than using the traditional mixing ventilation system (*MV*). For better understanding how to estimate this coil load, it was necessary to illustrate the airflow directions from/to the room and air handling unit, as illustrated in Figure 4. As it could be deduced from Figure 4, the exhausted hot air is drawn up from the exhaust vent in the center of the ceiling to leave the room. The return air from the selected return vent height is directed out from the room to be mixed with the fresh hot air from the outdoors, which compensates for the reduction in the flow rate by the exhausted air portion. Thereafter, the air mixture is cooled through the AHU coil and supplied to the room through the IJV supply duct, and, consequently, it is impinged to the room's floor to be distributed for comfortable cooling purposes.
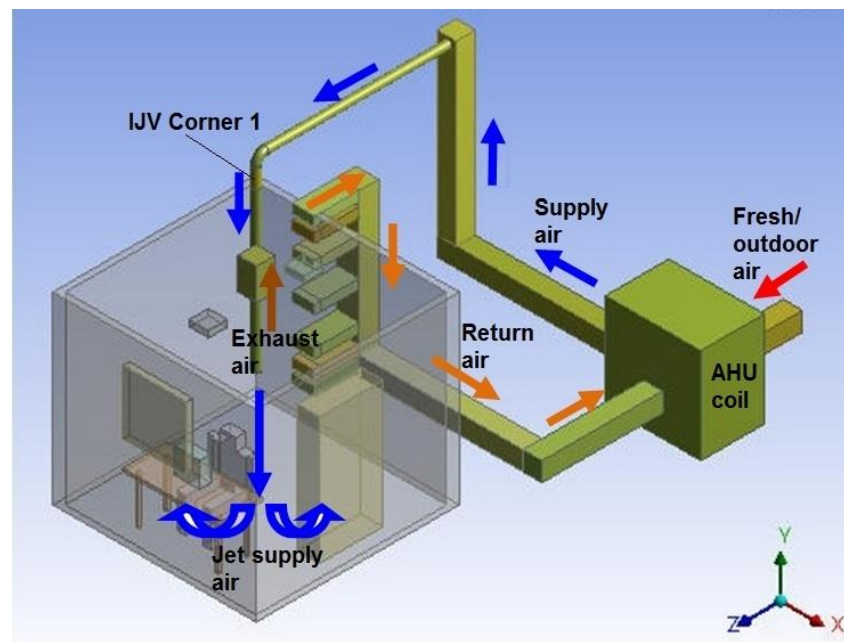
Figure 4. Air flow directions from/to room with connections to the air handling unit (AHU) coil, showing different return vent heights for the case of corner 1 supply air location.

The saving-energy potential term "ΔQ_{coil}" is frequently defined and used by previous researchers [17,22,34–36] as follows:

$$\Delta Q_{coil} = Q_{coil-MV} - Q_{coil-IJV} = \dot{m}_e \times c_p \times (T_e - T_{set}) \tag{1}$$

where $Q_{coil-MV}$ is the mixing ventilation coil load, $\dot{m}_e$ is the exhaust air mass flow rate, c_p is the air-specific heat capacity, T_e is the exhaust air temperature, and T_{set} is the set temperature in the space taken as 24 °C Qin et al. [20].

The exhaust air mass flow rate ($\dot{m}_e$) can be determined by applying mass balance across the room as follows:

$$\dot{m}_{total} = \dot{m}_s = \dot{m}_r + \dot{m}_e \tag{2}$$

where $\dot{m}_{total}$ is the total room-supplied air mass flow rate or $\dot{m}_s$, and $\dot{m}_r$ is the return air mass flow rate.

The last equation can be expressed in terms of the mass flow ratios as follows:

$$1 = \frac{\dot{m}_r}{\dot{m}_s} + \frac{\dot{m}_e}{\dot{m}_s} = \text{return air ratio} + \text{exhuast or fresh (outdoor) air ratio} \tag{3}$$

Generally, the air mass flow rate is calculated as a function of the air volume flow rate as follows:

$$\dot{m} = \rho \dot{V} \tag{4}$$

where ρ is the air density, and $\dot{V}$ is the air volume flow rate.

Energy saving is the main scope of the present study; however, it should not be the only parameter for the justification of related studies for HVAC purposes. For better justification, the energy saving should be coupled with other parameters from thermal and indoor air quality. In the following are specifications for such important other parameters.

4. Thermal Comfort and Air Quality Determinations

In the present study, the thermal comfort performance is justified between all studied cases using several key indices, as will be discussed in the following. The evaluation of these indices was focused on the local working zone which was set to 1 m^2 around the

manikin. For that purpose, eleven horizontal planes were constructed inside the local working zone and corresponding to heights of 0.1, 0.2, 0.3, 0.4, 0.5, 0.6, 0.7, 0.8, 0.9, 1.0, and 1.1 m. The average values of temperatures and velocities from the mentioned planes were employed to obtain the relevant data necessary for all coming thermal comfort indices.

4.1. Vertical Temperature Difference

The vertical temperature differential between the head and ankle levels is a main standard indicator for evaluating local thermal comfort. According to ASHRAE Standard 55-2020 [31], the temperature differential between a seating person's ankle level at 0.1 m above the floor and the head level at 1.1 m should not be more than 3 °C. This is computed as follows:

$$\Delta T_{Head-Ankel} = T_{1.1} - T_{0.1} \tag{5}$$

The evaluation of this index has significance due to the inherent characteristics of air stratification in the context of this particular ventilation system, unlike mixed ventilation, which tends to generate a less pronounced stratification in the working area, particularly during cooling mode by Ameen et al. [37].

4.2. Draught Rate (DR)

The *DR* is an additional metric that quantifies the level of distress experienced by an individual as a result of unwelcome cooling of the human body. The model forecasts the proportion of unhappiness resulting from drafts. The aforementioned index is determined by the variables of air velocity, temperature, and turbulence intensity. The calculation of *DR* is outlined in ISO 7730-2005 [15,38].

$$DR = (34 - T) \cdot (u - 0.05)^{0.62} \cdot (3.14 + 0.37 \cdot u \cdot I_l) \cdot$$
$$For \ u \ < \ 0.05 \ \text{m/s} \ use \ u \ = 0.05 \ \text{m/s} \tag{6}$$
$$For \ DR \ > 100\% \ take \ DR = 100\%$$

where *T* is the local air temperature, *u* is the mean air velocity, and I_l is the local turbulence intensity which can be obtained [15]:

$$I_l = \frac{100(2k)^{0.5}}{u} \tag{7}$$

k is turbulent kinetic energy (TKE).

ISO 7730-2005 [38] classifies temperature environments for *DR* into three categories. The best category is "A" with *DR* < 10%, followed by "B" with *DR* < 20%, and "C" with *DR* < 30%. In this research, *DR* is measured at ankle level (0.1 m above the floor).

4.3. PMV and PPD

Predicted mean vote (*PMV*) is a widely used metric for evaluating thermal comfort. The *PMV* model incorporates many variables, mainly including air temperature, mean radiant temperature, air velocity, relative humidity, metabolic rate, and garment insulation, in order to assess the thermal perception experienced by an individual inside a given work environment. According to ASHRAE 55-2020 [33], the term "*PMV*" is defined as a numeric scale ranging from −3 to +3, with −3 representing extremely cold, 0 being neutral, and +3 representing extremely hot. A *PMV* score of 0 signifies thermal neutrality, indicating that the environmental conditions are neither hot nor cold, resulting in thermal comfort for the individual. *PMV* is commonly assessed at a vertical distance of 1.1 m above the floor (at the level of the head) for an individual in a seating position. In this study, the *PMV* calculation is performed using a metabolic rate value of 1.0 MET that is estimated based on assumed person activity and a clothing level of 0.5 CLO. In all instances, the humidity value was established at 50%. The Predicted Percentage of Dissatisfied (*PPD*) is a quantitative metric that aims to estimate the proportion of individuals who experience thermal dissatisfaction due to excessive coolness or warmth. At a range of 5% *PPD*, the individual achieves thermal

equilibrium, which is represented by a *PMV* value of 0. A greater level of *PPD* indicates that the individual experiences either excessive cold or excessive heat. *PPD* is a function of *PMV*, as shown in the following [22].

$$PPD = 100 - 95 \cdot Exp - \left(0.03353 \cdot PMV^4 + 0.2179 \cdot PMV^2 \right) in\% \tag{8}$$

After collecting the relevant data, including the mean radiant temperature [28], the horizontal average mean air temperature and air velocity, and the MET and CLO values, the *PMV* and *PPD* findings were determined. The *PMV* is calculated using the online thermal comfort tool (Quadco Engineering PV [39]), while the *PPD* is calculated based on the aforementioned equation.

4.4. Mean Age of Air and Air Change Effectiveness

The air quality in an IJV is essentially assessed by calculating the average age of the air and measuring the efficacy of air changes (*ACE*). The local average age of air refers to the typical duration it takes for air to travel from the entrance of the supply inlet to a particular position inside the ventilated area. The following is the equation utilized to calculate the average age of air [40,41].

$$\frac{\partial}{\partial x_i}(\rho u_i \tau) = \frac{\partial}{\partial x_i} \cdot \left[\left(2.88\rho \cdot 10^{-5} + \frac{\mu_{eff}}{Sc_\tau} \right) \cdot \frac{\partial \tau}{\partial x_i} \right] + S_\tau \tag{9}$$

where μ_{eff} denotes the effective turbulent viscosity of air, τ indicates the local age of air, and Sc_τ signifies the turbulent Schmidt number associated with the age of air. The value of Sc_τ is 0.7. The source term S_τ is typically assigned a constant value of 1.0. The *ACE* metric was employed to assess the effectiveness of the IJV in introducing fresh air into the operational area. The term "*ACE*", air change effectiveness, refers to the ratio between the nominal time and mean age of air inside the working zone [21].

$$ACE = \frac{\tau_n}{\tau} \tag{10}$$

where τ_n and τ denotes in (s). The nominal time constant τ_n is defined as follows:

$$\tau_n = \frac{V_{room}}{q_i} \tag{11}$$

The variables V_{room} and q_i represent the room volume (m^3) and the intake supply air flow rate (m^3/s), respectively. A value of *ACE* equal to 1.0 signifies the presence of well-mixed air within the room. Based on the findings of ASHRAE [42] and Fan et al. [21], it is advised that the minimum acceptable value for the air change effectiveness (*ACE*) should be 0.95. This threshold is considered sufficient to ensure a satisfactory level of indoor air quality (IAQ) inside the working zone. Furthermore, a higher *ACE* value is indicative of improved indoor air quality.

5. Results and Discussions

Although the main scope of the present study is directed to the energy-saving potential, it is quite important at first to include discussions about thermal comfort and indoor air quality. Thus, the first part of this section will cover the results from the thermal comfort and air quality indices, describing which design is close to the recommended standards of thermal comfort. The second part will present a full analysis of the energy saving and the conclusions.

5.1. Thermal Comfort and Indoor Air Quality Indices

Figure 5a–g shows the results of averaged temperatures from horizontal planes at different heights from 0.1 m above the floor to 1.1 m inside the local working zone for

all studied simulations. The first observation from Figure 5 is that for all studied return vent heights the temperature levels are increasing along with the height of the room. This temperature level trend is varied according to the IJV location, as it is more pronounced for the corner 2 IJV location than midwall 1, midwall 2, and corner 1, respectively. This emphasizes the thermal stratification associated with the use of the IJV systems. It should be noted that, for most studied cases, this temperature gradient is highly ranged between 0.1 m and 0.7 m of the room height, while this gradient is decayed in the range between 0.7 and 1.1 m. Also, it can be shown from Figure 5 that some changes in these temperature stratifications are recorded with the varying of the return vent height. As an example, from Figure 5a of return height (rH) 2.9 m for the corner 2 location, the temperature changed from 24.19 °C at ankle level to 25.73 °C at head level. Figure 5g shows the same location of corner 2 but at a return vent height of 0.5 m, where the temperature changes from 24 to 25.93 °C.

The temperature stratification may be further quantified by determining the absolute temperature differential between the positions of the head and ankle (1.1–0.1 m), as seen in Figure 6. The diagram also illustrates the uppermost threshold that ASHRAE Standard 55-2020 [31] permits for temperature variation, which is 3 °C.

The findings indicate that the temperature variations seen in all situations are below the ASHRAE limit, around (~1 °C). These findings align with prior studies on the phenomenon of temperature stratification in cooling mode caused by impinging jet ventilation [15,37]. When comparing the temperature difference between different locations, it could be observed from Figure 6 that corner 2 locations report the highest temperature difference with about 1.6 °C, while the corner 1 location is reporting the lowest temperature difference.

The evaluation of the draught rate (*DR*: Equation (12)) at ankle level (H = 0.1 m) is illustrated in Figure 7. The results displayed that the *DR* levels for all studied cases were below the ISO 7730-2005 [38] limit for category A, that is, 10%. It could be observed from Figure 7 that comparable values are reported for all studied cases with little increase for both corner 2 and corner 1 locations.

Figure 8 displays the *PMV* fluctuations at heights ranging from 0.1 to 1.1 m for all locations examined at three return heights of 2.9, 1.7, and 0.5 m. Based on the data shown in Figure 8, it can be inferred that the *PMV* levels observed in all instances were between the range of −0.3 to 0.4. The thermal comfort range specified by ASHRAE Standard 55-2020 [31] is within the permitted range of $-0.5 \leq PMV \leq +0.5$. The observed patterns in *PMV* data validate its impact through the temperature stratification depicted in Figure 5. At lower heights (H = 0.1), when the ventilation system supplies cold air, the *PMV* value often tends to be lower (*PMV* < 0), except at midwall 2. At higher heights, an increasing trend for the *PMV* is found. It is evident that examples located at corner 1 and midwall 1 exhibited better *PMV* values near zero, indicating that this particular site is more favorable compared to other places.

The findings of *PPD* (Equation (8)) are displayed in Figure 9 for all locations examined at three return heights of 2.9, 1.7, and 0.5 m. Upon assessing the levels of postpartum depression (*PPD*), the findings indicated that the majority of the cases examined fell below the threshold of 10% as specified by the ASHRAE Standard. This is considered a reasonable degree of thermal comfort for individuals. Furthermore, the *PPD* values exhibited an increase in several instances at higher elevations of H ≥ 0.5 m.

The air change effectiveness (*ACE*—Equation (10)) values at head level (H = 1.1 m) for all instances examined are depicted in Figure 10. The *ACE* value findings are frequently above the threshold of 1.0, indicating the system's efficiency under hot summer circumstances for all studied IJV locations.
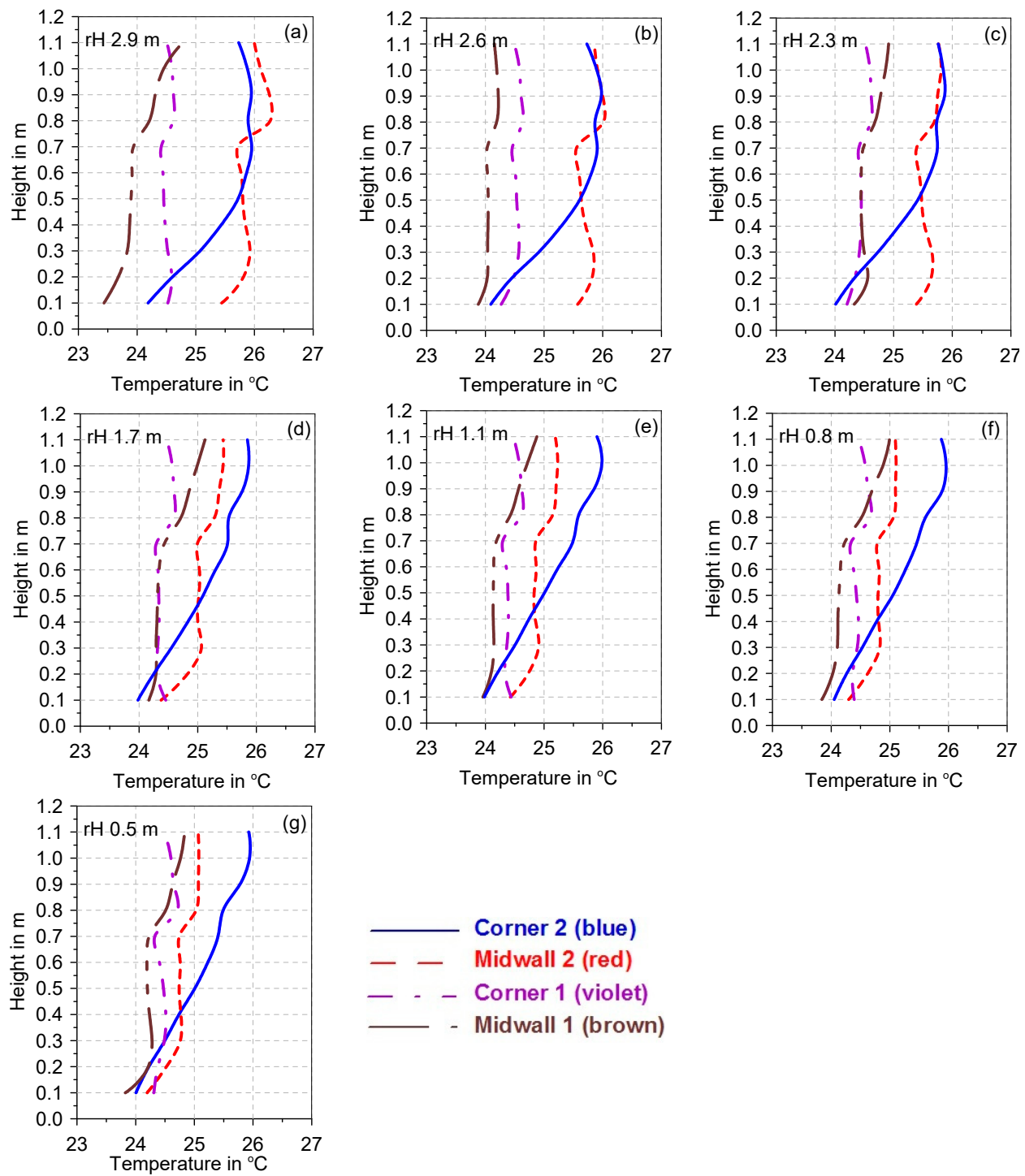
Figure 5. Averaged temperatures from horizontal planes at different heights in the local working zone for all studied simulations from height 0.1 m above the floor to 1.1 m; (**a**) rH = 2.9 m, (**b**) rH = 2.6 m, (**c**) rH = 2.3 m, (**d**) rH = 1.7 m, (**e**) rH = 1.1 m, (**f**) rH = 0.8 m, and (**g**) rH = 0.5 m.
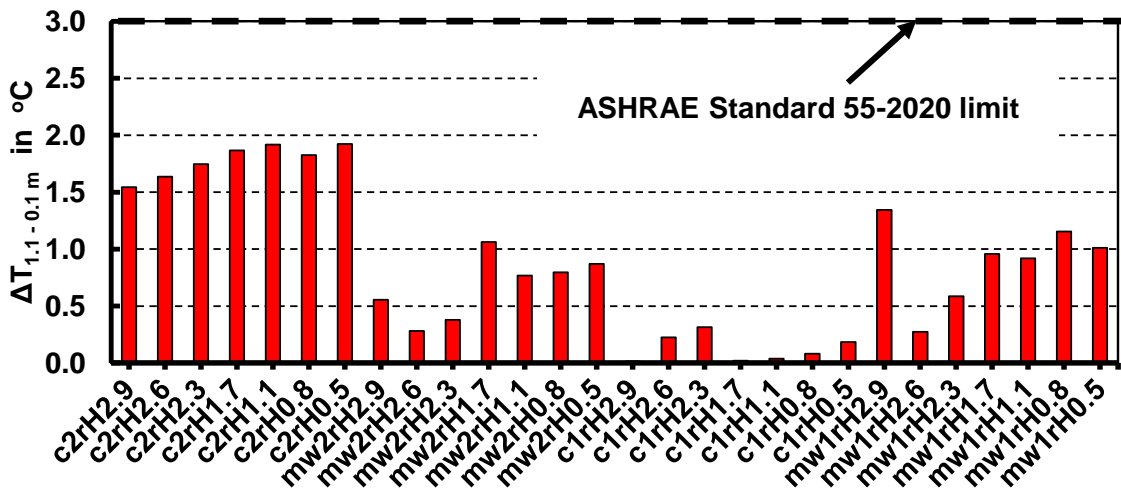
Figure 6. Absolute values of temperature difference among heights 1.1 and 0.1 m in the local comfort zone for all studied simulations.
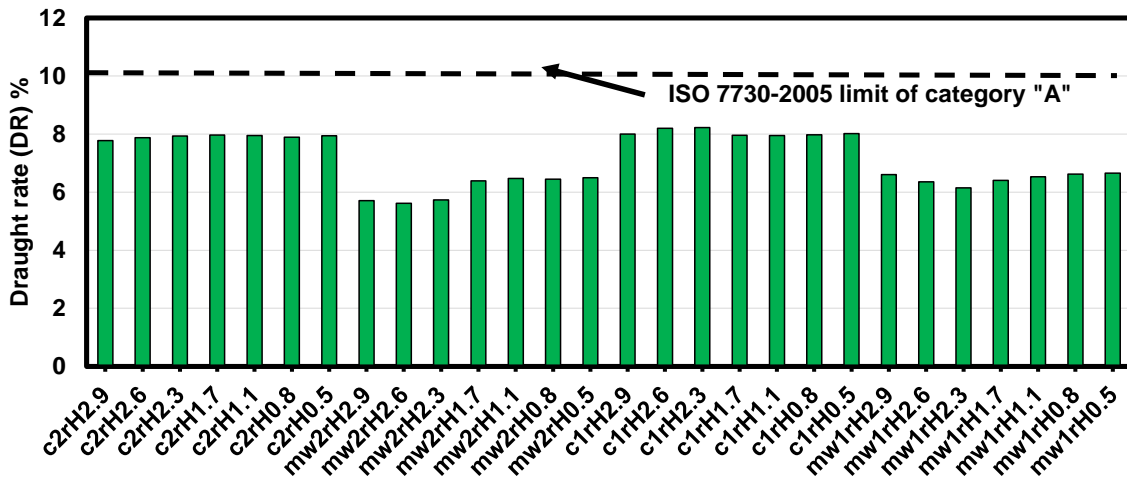

Figure 7. Draught rate (*DR*) percentage for all studied simulations was calculated at the ankle level (0.1 m above the floor).
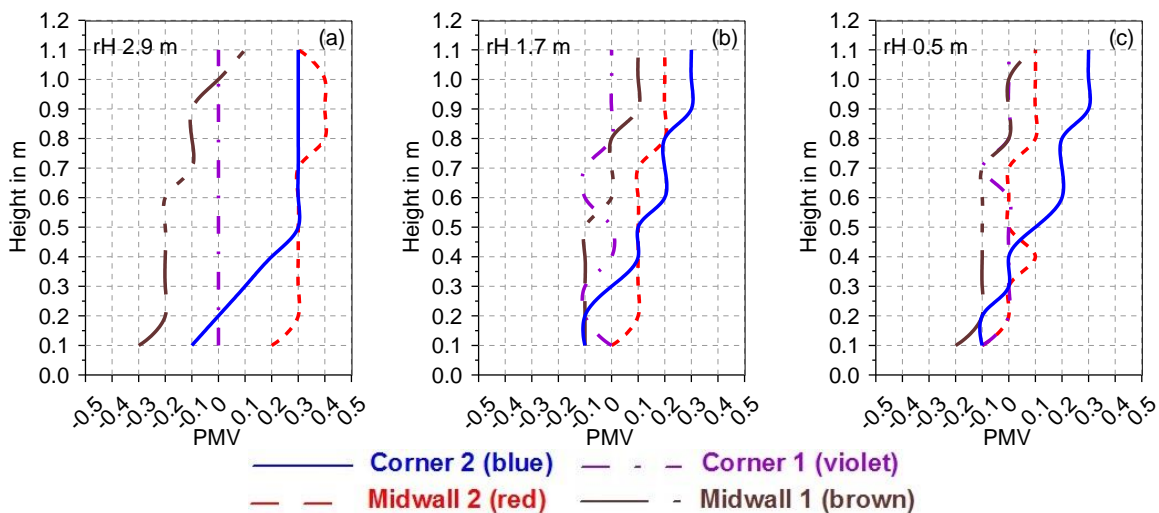
Figure 8. PMV variations with room height for all studied simulations from height 0.1 m above the floor to 1.1 m; (**a**) rH = 2.9 m, (**b**) rH = 1.7 m, and (**c**) rH = 0.5 m.
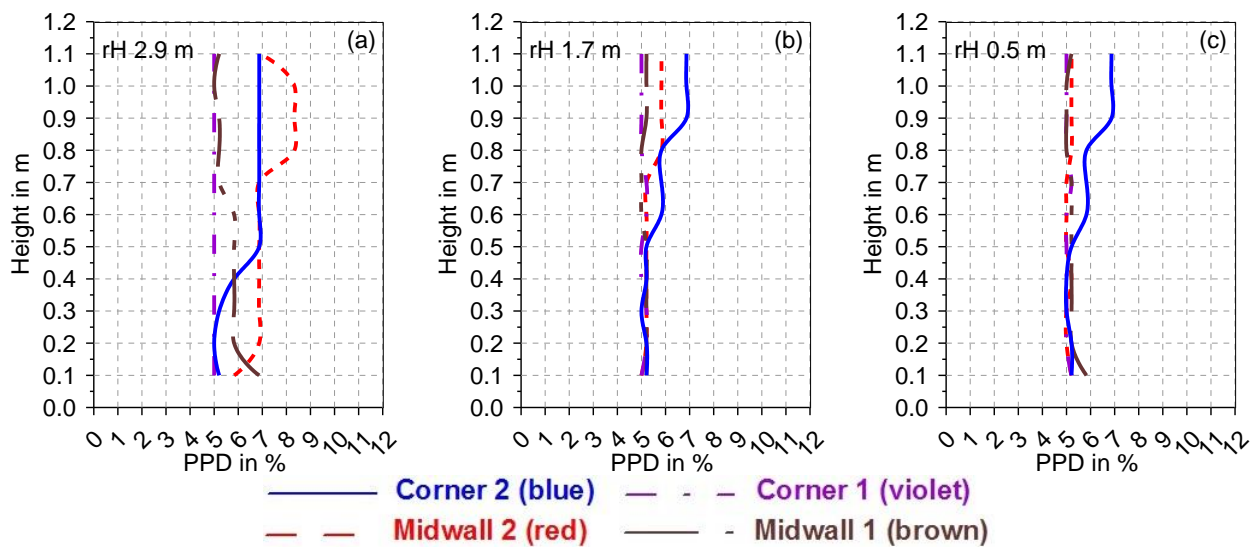
Figure 9. PPD variations with room height for all studied simulations from height 0.1 above the floor to 1.1 m; (**a**) rH = 2.9 m, (**b**) rH = 1.7 m, and (**c**) rH = 0.5 m.
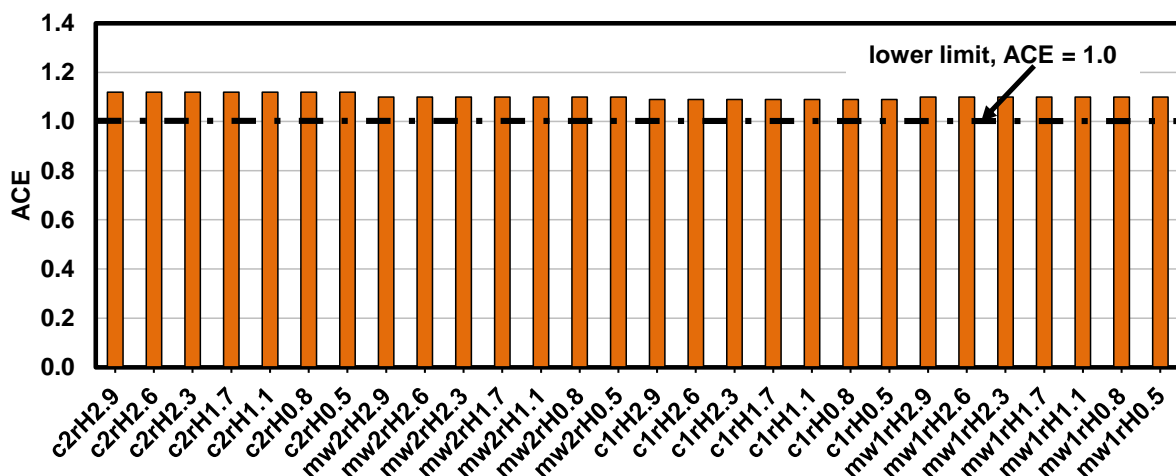

Figure 10. Air change effectiveness (*ACE*) for all studied simulations was calculated at the head level (1.1 m above the floor).

For more clarifications and justification on the temperature and flow characteristics, Figures 11 and 12 can be used. Figure 11 shows temperature contours at room YZ mid-plane for all studied locations at three return vent heights of 2.9, 1.7, and 0.5 m. The main observation from Figure 11 is that decreasing the return vent height affected the temperature levels in the local working zone as well as increasing the exhaust air temperature.

Figure 12 shows streamlines at room YZ mid-plane for all studied locations at a return vent height of 1.7 m. The results from Figure 12 showed the formation of large vortex regions in many positions in the room for all IJV locations except the midwall 1 location. The midwall 1 location (IJV in the midwall behind the person and far from the hot exterior wall) reports much-enhanced flow characteristics with even no vortex formation, especially inside the local working zone.

At the end of this part, it could be concluded that corner 1 and midwall 1 locations exhibit better thermal comfort characteristics when compared to corner 2 and midwall 2 locations. However, the midwall 1 location showed enhanced flow characteristics over other studied locations. A conclusion can be drawn after the discussion from the energy-saving part.
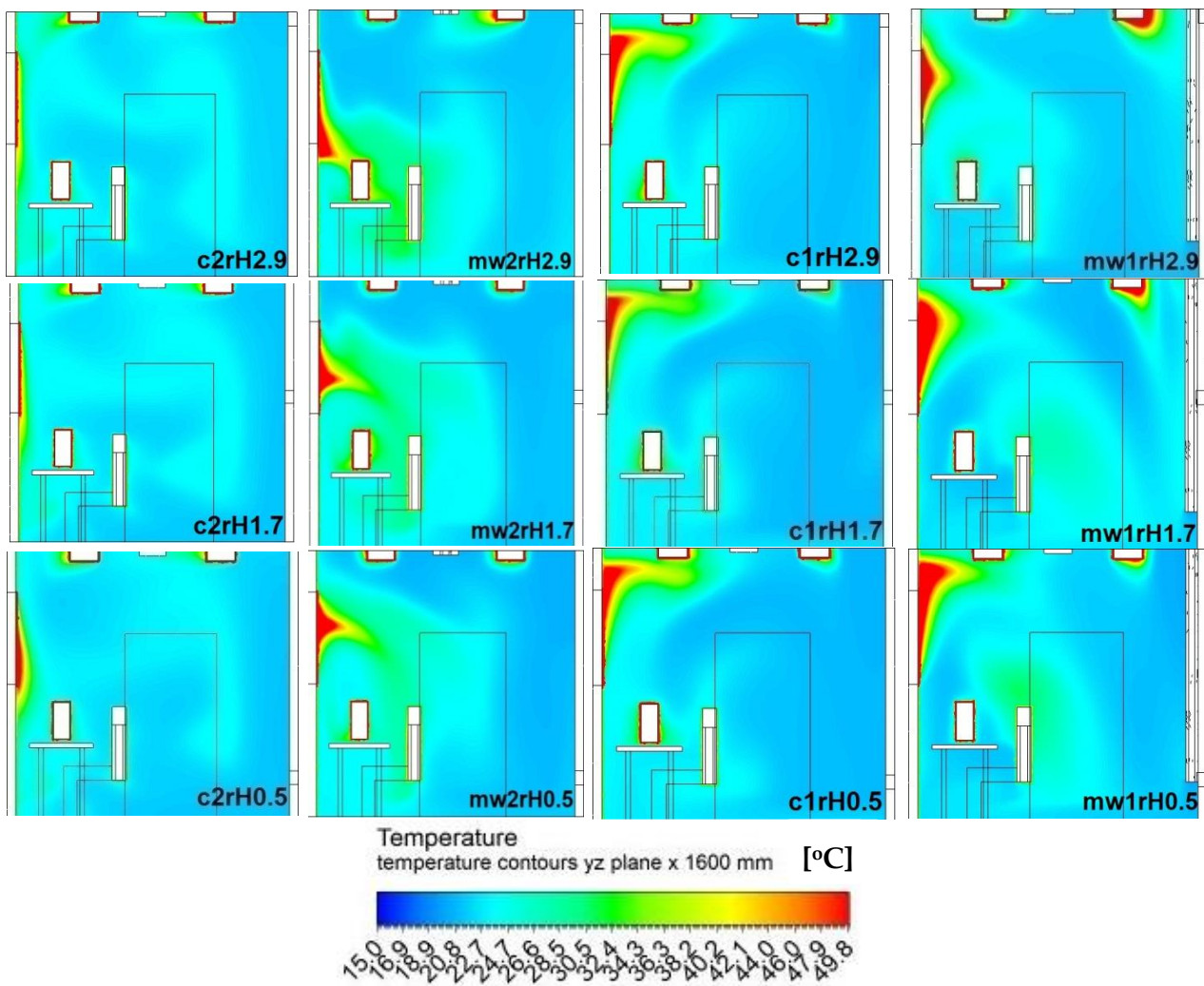
Figure 11. Temperature contours at room YZ mid-plane for some studied cases. c: corner; mw: midwall; and rH: return height in m.
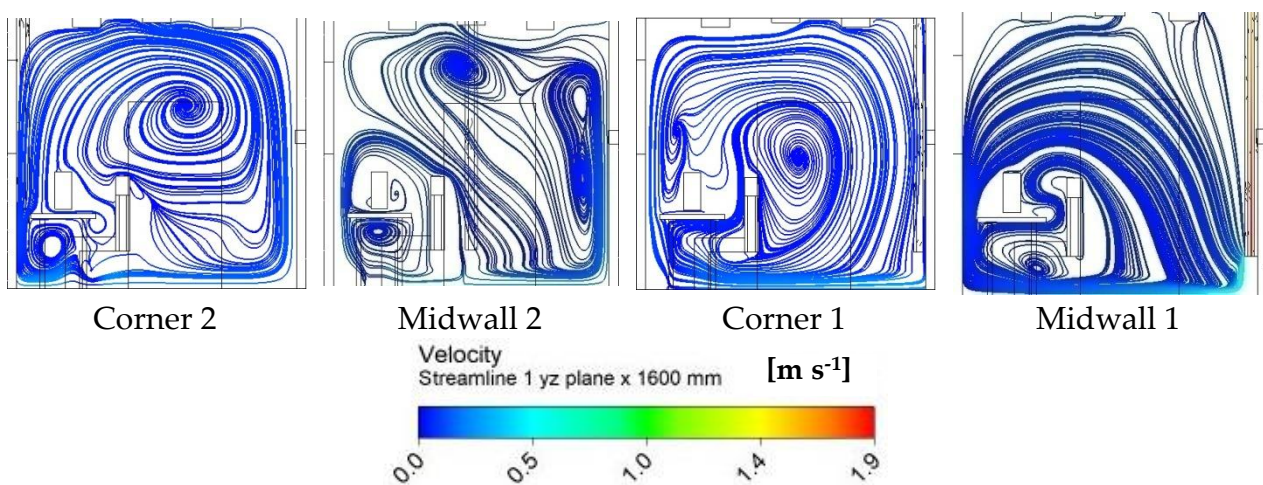

Figure 12. Velocity streamlines at room YZ mid-plane for some studied cases at a return height of rH = 1.7 m.

5.2. Energy-Saving Potential

From Equation (1) it could be deduced that the higher the positive value of ΔQ_{coil}, the higher the energy saving is expected when using the IJV system rather than using the MV system. Also, it could be understood that ΔQ_{coil} depends on two parameters: the exhausted air portion flow rate ($\dot{m}_e$) and the exhausted air temperature (T_e). But, since the exhaust air portion flow rate is constant here, ΔQ_{coil} will be dominant by the exhaust air temperature. Thus, higher exhaust air temperatures are targeted to achieve higher energy saving as possible. This can demonstrate the best choice of the exhaust vent to be located in the center of the ceiling [43] between the two lighting systems and just above the local thermal plume. Another important parameter in determining the required individual coil load is the returned air temperature. As per common sense, the lower the return temperature, the lower the required individual coil load for the same supplied air and outdoor conditions, where this aimed decrease in the return air temperature is pronounced by lowering the return vent height, but with care to avoid "short-circuiting" at a very low vent height that is close to the IJV supply height (0.4 m). Figure 13 illustrates the energy-saving potential for all studied cases. One important note that could be deduced from Figure 13 is that the energy-saving common trend for all IJV locations increased as the return vent height decreased except for little odd cases from corner 2 and midwall 2. This common trend is expected due to the decrease in the return air temperature. Another reason is the higher exhaust temperature reported, while little odd trends are reported for the nearest IJV locations to the exterior wall, corner 2, and midwall 2, in order. These locations reported high exhaust air temperatures at higher return vent heights. Also, it could be deduced from Figure 13 that for most studied cases, the lowest vent height at 0.5 m reports a slightly lower energy saving than the height of 0.8 m, which is also opposite the common trend. At this lowest vent height, the danger from the short circuit begins. Based on this, it can be recommended to avoid lower vent heights than 0.8 m, or to make the return vent height between 1.7 and 0.8 m. Similar conclusions are found in previous studies [17,21]. As an example, from the results in Figure 13 for the case of the corner 1 location, the ΔQ_{coil} increases by about 20% when the return vent height is lowered from 2.9 m to 0.8 m, while a little decrease is reported by about 7% after the return vent height reaches 0.5 m. Also, it could be reported from Figure 13 that the lowest values of energy saving are reported for the midwall 2 location. As a result, it is recommended to exclude the midwall 2 location from use in such applications. The other three locations showed comparable values, while noting the odd trends for some cases from the corner 2 location as discussed earlier, which can also make this location excluded from use.
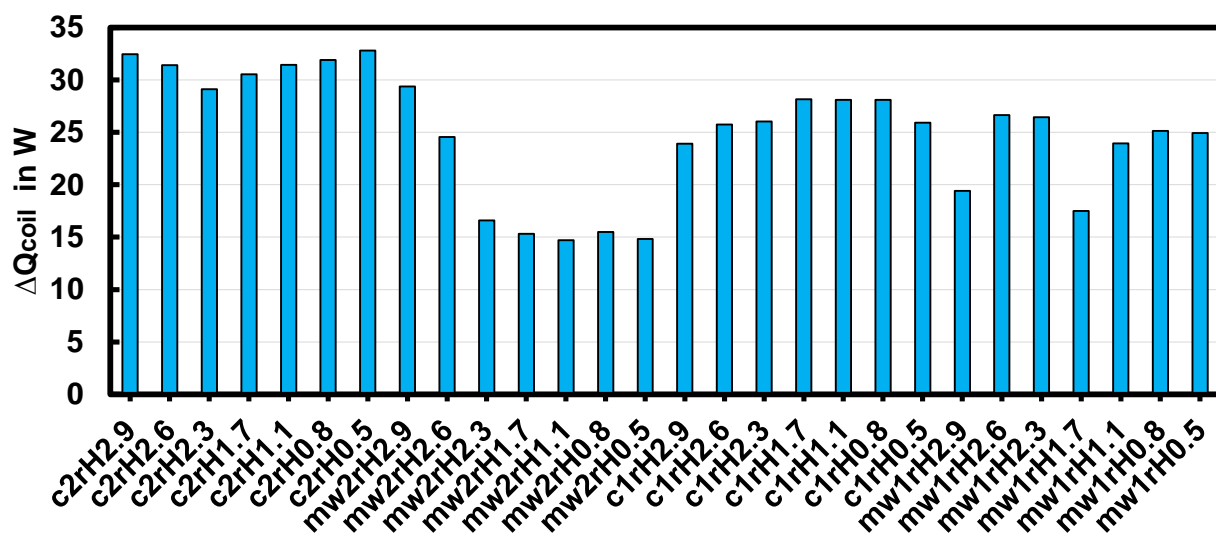

Figure 13. Energy-saving potential for all studied cases.

Finally, what should be importantly mentioned regarding the results of the ΔQ_{coil} is that the reported values are somewhat modest. This implies little significance in using IJV systems rather than MV systems from the energy-saving point of view. This cannot be the case because the present study is considering a small office room with an adequate low supply air flow rate (75 m^3/h) with a small exhaust air flow ratio (17%). However, when the application is larger, the supplied air flow rate will also be larger, which in turn increases the energy-saving potential and consequently the significance of using the IJV systems. Gathering the data from the two parts, thermal comfort and flow characteristics, besides energy saving, it can be generally confirmed preferable to use the locations of midwall 1, which is behind the seated person and far from the exterior hot wall, and which is also characterized by low vortex formation, especially in the local working zone. This helps for a much more comfortable sensation in the persons. A similar recommendation for using the midwall 1 location was reported by a few researchers with the minimum information for the justification [30].

6. Conclusions

In this work, many CFD simulations are carried out to simulate the real environment of an office building (3 × 3 × 2.9 m^3) for the cooling mode in the hot summer climate. The room contains one seated thermal manikin and is furnished with a chair, a desk, a personal computer, and a cupboard. Two lighting systems are installed in the ceiling. The room has only one side wall that includes a glass window of 1 m^2 area and faces the exterior ambient conditions outside the building at 38 °C outdoor temperature and 700 W/m^2 solar irradiation, while the remaining internal five walls including the floor and the ceiling are assumed adiabatic. The height of the IJV system air inlet to the room is kept at 0.4 m. The air inlet-to-room conditions coming from the IJV were kept constant at 20 °C, 75 m^3/h, and 50% relative humidity. In the present study, the exhaust vent is separated from the return vent. The exhaust vent is located at the center of the ceiling. Seven return vent heights are examined at 2.9, 2.6, 2.3, 1.7, 1.1, 0.8, and 0.5 m from the floor. Four different locations of the IJV system with meaningful purposes such as nice decoration and good interior design have been selected in the current study: two corners and two midwalls, for a fixed-person position: corner 1 (behind manikin), corner 2 (front of manikin), midwall 1 (behind manikin), and midwall 2 (right side of manikin). A full 3D CFD model without using any symmetrical boundary conditions is investigated to study the effect of IJV location and return vent height on the energy-saving potential and thermal comfort indices. The RNG k–ε turbulence model is used with enhanced wall treatment.

The results from the current study recommended that the best range for the return vent height is between 1.7 and 0.8 m. A return vent height lower than 0.8 m should not be used to avoid the problems of short-circuiting. Also, it is recommended to use the IJV locations far from the hot exterior wall. Finally, by gathering the data from the two parts, thermal comfort and flow characteristics, besides energy saving, it can be confirmed to use the midwall 1 location. It yields low vortex formation, especially in the local working zone, which helps for a much more comfortable sensation besides good energy-saving potential.

This article, alongside existing literature, offers valuable insights for HVAC designers in this field of study. Future studies on improving the nonuniform environment associated with using IJV systems and based on the recommended IJV location from the present study are interesting.

Nomenclature

C_1–C_3	constants in Equation (6)
D	diameter, mm
G_b	the kinetic energy of turbulence rate to buoyancy, J/kg·s
G_k	kinetic energy rate of turbulence to mean velocity gradients, J/kg·s
H	height, m
I_l	local turbulence intensity, %
k	turbulent kinetic energy, J/kg
$\dot{m}$	mass flow rate, kg/s
Q	heat transfer rate, W
q_i	the inlet supply air flow rate, m^3/s
t	time, sec
T	local temperature, K
u	velocity, m/s
u'	fluctuating velocity, m/s
V	volume, m^3
$\dot{V}$	volume flow rate, m^3/s

Abbreviations

ACE	air change effectiveness
AHU	air handling unit
ASHRAE	American Society of Heating, Refrigerating, and Air-Conditioning Engineers
CFD	computational fluid dynamics
COP	coefficient of performance
DR	draught rate, %
DV	displacement ventilation
HVAC	heating, ventilation, and air conditioning
IJV	impinging jet ventilation
IQA	indoor air quality
MV	mixing ventilation
PMV	predicted mean vote
PPD	Predicted Percentage of Dissatisfied, %
RANS	Reynolds-averaged Navier–Stokes
RH	relative humidity
RMS	residual mean square
TKE	turbulent kinetic energy
ΔQ_{coil}	energy-saving potential

Subscripts

e	exhaust
o	outdoor
r	return
s	supply

Greek Letters

ρ	fluid density, kg/m^3
δ_{ij}	Kronecker delta, dimensionless
τ_n	nominal time constant, sec
τ	arithmetic average age of air, sec
Δ	difference
μ	fluid dynamic viscosity, Pa·s
μ_t	turbulent viscosity, kg/(m·s)
ε	dissipation rate, m^2/s^3

References

1. Alajmi, A.; El-Amer, W. Saving energy by using underfloor-air-distribution (UFAD) system in commercial buildings. *Energy Convers. Manag.* **2010**, *51*, 1637–1642. [CrossRef]
2. Yang, B.; Liu, P.; Liu, Y.; Jin, D.; Wang, F. Assessment of thermal comfort and air quality of room conditions by impinging jet ventilation integrated with ductless personalized ventilation. *Sustainability* **2022**, *14*, 12526. [CrossRef]
3. Zhou, B.; Li, Z.; Yang, B.; Li, X.; Wang, F.; Wei, S. Thermal and draught perception in fluctuating stratified thermal environments with intermittent impinging jet ventilation. *Build. Environ.* **2023**, *229*, 109934. [CrossRef]
4. Karimipanah, T.; Awbi, H.B. Theoretical and experimental investigation of impinging jet ventilation and comparison with wall displacement ventilation. *Build. Environ.* **2002**, *37*, 132942. [CrossRef]
5. Awbi, H.B. *Ventilation of Buildings*; Spon Press: London, UK, 2003.
6. Rohdin, P.; Moshfegh, B. Numerical predictions of indoor climate in large industrial premises. A comparison between different k-ε models supported by field measurements. *Build. Environ.* **2007**, *42*, 3872–3882. [CrossRef]
7. Varodompun, J. Architectural and HVAC Applications of Impinging Jet Ventilation Using Full Scale and CFD Simulation. Ph.D. Thesis, University of Michigan, Ann Arbor, MI, USA, 2008.
8. Chen, H.; Moshfegh, B.; Cehlin, M. Computational investigation on the factors influencing thermal comfort for impinging jet ventilation. *Build. Environ.* **2013**, *66*, 29–41. [CrossRef]
9. Yuan, X.X.; Chen, Q.Y.; Glicksman, L.R. Acritical review of displacement ventilation. *ASHRAE Trans.* **1998**, *104*, 78–90.
10. Melikov, A.K.; Langkilde, G.; Derbiszewski, B. Air flow characteristics in the occupied zone of rooms with displacement ventilation. *ASHRAE Trans.* **1990**, *96*, 63–555.
11. Chen, H.; Moshfegh, B.; Cehlin, M. Numerical investigation of the flow behavior of an isothermal impinging jet in a room. *Build. Environ.* **2012**, *49*, 154–166. [CrossRef]
12. Varodompun, J.; Navvab, M. HVAC ventilation strategies: The contribution for thermal comfort, energy efficiency, and indoor air quality. *J. Green Build.* **2007**, *2*, 50–131. [CrossRef]
13. Staveckis, A.; Borodinecs, A. Impact of impinging jet ventilation on thermal comfort and indoor air quality in office buildings. *Energy Build.* **2021**, *235*, 110738. [CrossRef]
14. Hu, J.; Kang, Y.; Lu, Y.; Yu, J.; Li, H.; Zhong, K. Numerical investigation of the thermal and ventilation performance of a combined impinging jet ventilation and passive chilled beam system. *Build. Environ.* **2022**, *226*, 109726. [CrossRef]
15. Chen, H.; Moshfegh, B.; Cehlin, M. Investigation on the flow and thermal behavior of impinging jet ventilation systems in an office with different heat loads. *Build. Environ.* **2013**, *59*, 127–144. [CrossRef]
16. Cehlin, M.; Karimipanah, T.; Larsson, U.; Ameen, A. Comparing thermal comfort and air quality performance of two active chilled beam systems in an open-plan office. *J. Build. Eng.* **2019**, *22*, 56–65. [CrossRef]
17. Cheng, Y.; Yang, J.; Du, Z.; Peng, J. Investigations on the energy efficiency of stratified air distribution systems with different diffuser layouts. *Sustainability* **2016**, *8*, 732. [CrossRef]
18. Haghshenaskashani, S.; Sajadi, B. Evaluation of thermal comfort, IAQ and energy consumption in an impinging jet ventilation (IJV) system with/without ceiling exhaust. *J. Build. Eng.* **2018**, *18*, 142–153. [CrossRef]
19. Ahmed, A.Q.; Gao, S.; Kareem, A.K. A numerical study on the effects of exhaust locations on energy consumption and thermal environment in an office room served by displacement ventilation. *Energy Convers. Manag.* **2016**, *117*, 74–85. [CrossRef]
20. Qin, C.; Wu, S.-H.; Fang, H.-Q.; Lu, W.-Z. The impacts of evaluation indices and normalization methods on E-TOPSIS optimization of return vent height for an impinging jet ventilation system. *Build. Simul.* **2022**, *15*, 2081–2095. [CrossRef]
21. Fan, Y.; Li, X.; Yan, Y.; Tu, J. Overall performance evaluation of underfloor air distribution system with different heights of return vents. *Energy Build.* **2017**, *147*, 176–187. [CrossRef]
22. Qin, C.; Lu, W.-Z. Effects of ceiling exhaust location on thermal comfort and age of air in room under impinging jet supply scheme. *J. Build. Eng.* **2021**, *35*, 101966. [CrossRef]
23. Yakhot, V.; Orszag, S.A. Renormalization group analysis of turbulence. I. Basic theory. *J. Sci. Comput.* **1986**, *1*, 3–51. [CrossRef]
24. Ye, X.; Kang, Y.; Yang, F.; Zhong, K. Comparison study of contaminant distribution and indoor air quality in large-height spaces between impinging jet and mixing ventilation systems in heating mode. *Build. Environ.* **2019**, *160*, 106159. [CrossRef]
25. Hu, J.; Kang, Y.; Lu, Y.; Yu, J.; Zhong, K. Simplified models for predicting thermal stratification in impinging jet ventilation rooms using multiple regression analysis. *Build. Environ.* **2021**, *206*, 108311. [CrossRef]
26. Hu, J.; Kang, Y.; Yu, J.; Zhong, K. Numerical study on thermal stratification for impinging jet ventilation system in office buildings. *Build. Environ.* **2021**, *196*, 107798. [CrossRef]
27. Ameen, A.; Cehlin, M.; Larsson, U.; Yamasawa, H.; Kobayashi, T. Numerical investigation of the flow behavior of an isothermal corner impinging jet for building ventilation. *Build. Environ.* **2022**, *223*, 109486. [CrossRef]
28. Ameen, A.; Cehlin, M.; Yamasawa, H.; Kobayashi, T.; Karimipanah, T. Energy saving, indoor thermal comfort and indoor air quality evaluation of an office environment using corner impinging jet ventilation. *Dev. Built Environ.* **2023**, *15*, 100179. [CrossRef]
29. Yang, B.; Liu, P.; Liu, Y.; Wang, F. Performance evaluation of ductless personalized ventilation combined with impinging jet ventilation. *Appl. Therm. Eng.* **2023**, *222*, 119915. [CrossRef]
30. Yamasawa, H.; Kobayashi, T.; Yamanaka, T.; Choi, N.; Cehlin, M.; Ameen, A. Effect of supply velocity and heat generation density on cooling and ventilation effectiveness in room with impinging jet ventilation system. *Build. Environ.* **2021**, *205*, 108299. [CrossRef]

31. *ANSI/ASHRAE Standard 55-2020*; Thermal Environmental Conditions for Human Occupancy. American Society of Heating and Refrigerating and Air-Conditioning Engineers: Atlanta, GA, USA, 2021.

32. Karali, M.A.; Almohammadi, B.A.; Bin Mahfouz, A.S.; Abdelmohimen, M.A.; Attia, E.-A.; Refaey, H. Effect of surfaces roughness of a staggered tube bank in cross flow with air on heat transfer and pressure drop. *Case Stud. Therm. Eng.* **2023**, *43*, 102779. [CrossRef]

33. ANSYS Inc. *ANSYS CFX-Solver Theory Guide*; R18.0; ANSYS Inc.: Canonsburg, PA, USA, 2017.

34. Wei, D.; Zuo, M.-X.; Yu, J. Control strategy for energy saving of refrigerating station systems in public buildings. *J. Build. Eng.* **2021**, *44*, 103198. [CrossRef]

35. Hussain, S.A.; Wang, L.; Huang, P.; Sadiq, R.; Hewage, K. Dissimilarity-driven ensemble model-based real-time optimization for control of building HVAC systems. *J. Build. Eng.* **2022**, *52*, 104376. [CrossRef]

36. Liang, C.; Li, X.; Shao, X.; Li, B. Numerical analysis of the methods for reducing the energy use of air-conditioning systems in non-uniform indoor environments. *Build. Environ.* **2020**, *167*, 106442. [CrossRef]

37. Ameen, A.; Cehlin, M.; Larsson, U.; Karimipanah, T. Experimental Investigation of the Ventilation Performance of Different Air Distribution Systems in an Office Environment—Cooling Mode. *Energies* **2019**, *12*, 1354. [CrossRef]

38. *ISO 7730:2005*; Ergonomics of the Thermal Environment: Analytical Determination and Interpretation of Thermal Comfort Using Calculation of the PMV and PPD Indices and Local Thermal Comfort Criteria. ISO: Geneva, Switzerland, 2005.

39. Quadco Engineering PV Online Thermal Comfort Tool. Available online: https://www.quadco.engineering/en/know-how/cfd-calculate-pmv-and-ppd.htm (accessed on 13 April 2024).

40. Li, X.; Li, D.; Yang, X.; Yang, J. Total air age: An extension of the air age concept. *Build. Environ.* **2003**, *38*, 1263–1269. [CrossRef]

41. Ye, X.; Kang, Y.; Yan, Z.; Chen, B.; Zhong, K. Optimization study of return vent height for an impinging jet ventilation system with exhaust/return-split configuration by TOPSIS method. *Build. Environ.* **2020**, *177*, 106858. [CrossRef]

42. *ASHRAE Standard 129*; AS Measuring Air-Change Effectiveness. AHSRAE: Corners, GA, USA, 1997.

43. Hu, J.; Kang, Y.; Lu, Y.; Yu, J.; Zhong, K. A simple method and prediction model for calculating the cooling load of impinging jet ventilation system in office buildings. *Build. Environ.* **2024**, *254*, 111408. [CrossRef]